SCIENCE CHINA PRESS

SCIENCE CHINA Life Sciences
life.scichina.com link.springer.com
https://doi.org/10.1007/s11427-024-2818-7

COVER ARTICLE

Peri-centrosomal localization of small interfering RNAs in *C. elegans*

Qile Jin[1†], Xuezhu Feng[2†], Minjie Hong[1], Ke Wang[1], Xiangyang Chen[1], Jiewei Cheng[1], Yan Kuang[1], Xiaoyue Si[1], Mingjing Xu[1], Xinya Huang[1*], Shouhong Guang[1*] & Chengming Zhu[1*]

[1]Department of Obstetrics and Gynecology, The First Affiliated Hospital of USTC, The USTC RNA Institute, Ministry of Education Key Laboratory for Membraneless Organelles & Cellular Dynamics, Hefei National Research Center for Physical Sciences at the Microscale, Center for Advanced Interdisciplinary Science and Biomedicine of IHM, School of Life Sciences, Division of Life Sciences and Medicine, Biomedical Sciences and Health Laboratory of Anhui Province, University of Science and Technology of China, Hefei 230027, China
[2]School of Basic Medicine, Anhui Medical University, Hefei 230032, China

†Contributed equally to this work
*Corresponding authors (Xinya Huang, email: hxy1996@ustc.edu.cn; Shouhong Guang, email: sguang@ustc.edu.cn; Chengming Zhu, email: zcm916@ustc.edu.cn)

Received 7 October 2024; Accepted 16 December 2024; Published online 14 January 2025

The centrosome is the microtubule-organizing center and a crucial part of cell division. Centrosomal RNAs (cnRNAs) have been reported to enable precise spatiotemporal control of gene expression during cell division in many species. Whether and how cnRNAs exist in *C. elegans* are unclear. Here, using the nuclear RNAi Argonaute protein NRDE-3 as a reporter, we observed potential peri-centrosome localized small interfering (si)RNAs in *C. elegans*. NRDE-3 was previously shown to associate with pre-mRNAs and pre-rRNAs via a process involving the presence of complementary siRNAs. We generated a GFP-NRDE-3 knock-in transgene through CRISPR/Cas9 technology and observed that NRDE-3 formed peri-centrosomal foci neighboring the tubulin protein TBB-2, other centriole proteins and pericentriolar material (PCM) components in *C. elegans* embryos. The peri-centrosomal accumulation of NRDE-3 depends on RNA-dependent RNA polymerase (RdRP)-synthesized 22G siRNAs and the PAZ domain of NRDE-3, which is essential for siRNA binding. Mutation of *eri-1*, *ergo-1*, or *drh-3* significantly increased the percentage of pericentrosome-enriched NRDE-3. At the metaphase of the cell cycle, NRDE-3 was enriched in both the peri-centrosomal region and the spindle. Moreover, the integrity of centriole proteins and pericentriolar material (PCM) components is also required for the peri-centrosomal accumulation of NRDE-3. Therefore, we concluded that siRNAs could accumulate in the peri-centrosomal region in *C. elegans* and suggested that the peri-centrosomal region may also be a platform for RNAi-mediated gene regulation.

siRNA | centrosomal RNAs | NRDE-3

INTRODUCTION

Centrosomes are nonmembrane organelles. The core of the centrosome consists of a pair of orthogonally oriented centrioles surrounded by a dynamic assembly of proteins known as the pericentriolar material (PCM). Centrosomes are responsible for microtubule nucleation and organization, spindle assembly, cell division, and cell polarity (Pintard and Bowerman, 2019).

Centrosomal RNAs (cnRNAs) were identified by studying the oocytes of the surf clam (*Spisula solidissima*) as early as 2006 (Alliegro et al., 2006). Scientists have used purification methods and labeling approaches to discover cnRNAs. With the development of new technologies, localization-based approaches such as single molecular FISH (smFISH) and transcriptomic approaches such as single-cell sequencing have accelerated the characterization of cnRNAs (Zein-Sabatto and Lerit, 2021). Centrosomal RNAs have since been identified in diverse model systems, including *Ilyanassa*, *Spisula*, *Drosophila*, *Xenopus*, zebrafish, mollusk, and mammalian cell lines (Alliegro and Alliegro, 2008; Alliegro et al., 2006; Bergalet et al., 2020; Blower et al., 2007; Lambert and Nagy, 2002; Lécuyer et al., 2007; Raff et al., 1990; Sepulveda et al., 2018), suggesting that the localization of mRNAs to the centrosome is an evolutionarily conserved phenomenon. However, it is unclear whether and how cnRNAs exist in *C. elegans*.

Centrosomal RNAs are proposed to have three main functions. First, RNAs localize to the centrosome to regulate centrosome function and mitotic integrity via co-translational mechanisms. Since cell division is a highly dynamic process, cnRNAs and co-translational centrosome proteins may effectively respond to cell cycle demands (Lerit, 2022). Mislocalized cnRNAs have been shown to disrupt microtubule organization and induce mitotic errors (Fang and Lerit, 2022; Ryder et al., 2020). Second, asymmetrically localized cnRNAs may contribute to asymmetric cell division and lead to embryonic patterning and selective inheritance of specific transcripts (Bergalet et al., 2020; Lambert and Nagy, 2002; Safieddine et al., 2021; Sepulveda et al., 2018). Third, cnRNAs may support the structural integrity of centrosomes and promote phase separation within the centrosome (Ryder and Lerit, 2018).

Citation: Jin, Q., Feng, X., Hong, M., Wang, K., Chen, X., Cheng, J., Kuang, Y., Si, X., Xu, M., Huang, X., et al. Peri-centrosomal localization of small interfering RNAs in *C. elegans*. Sci China Life Sci, https://doi.org/10.1007/s11427-024-2818-7

RNA interference (RNAi) is a conserved mechanism that silences complementary mRNAs via Argonaute/siRNA complexes at the posttranscriptional level (Fire et al., 1998). siRNAs are generated by the conserved ribonuclease Dicer and bound by Argonaute (Ago) proteins to degrade targeted RNA or inhibit its translation (Bernstein et al., 2001; Billi et al., 2014; Castel and Martienssen, 2013). In addition, in many organisms, RNA-dependent RNA polymerases (RdRPs) can synthesize secondary siRNAs to amplify silencing signals (Cogoni and Macino, 1999; Pak and Fire, 2007). In *C. elegans*, siRNAs silence nucleus-localized RNAs via the nuclear RNAi defective (Nrde) pathway (Guang et al., 2010; Guang et al., 2008). The somatic nuclear Argonaute NRDE-3, or HRDE-1 in the germline, transports 22G siRNAs from the cytoplasm to the nucleus, where they bind to nascent transcripts and recruit other NRDE factors to inhibit RNA polymerase I/II elongation and induce H3K9 and H3K27 trimethylation (Fischer and Ruvkun, 2020; Guang et al., 2010; Mao et al., 2015; Padeken et al., 2021). NRDE-3 has been used to reveal tissue-specific gene expression (Guang et al., 2008), antisense ribosomal siRNAs (risiRNAs) (Liao et al., 2021; Zhou et al., 2017), and transcriptional dynamics *in vivo* (Barrière and Bertrand, 2022; Toudji-Zouaz et al., 2021).

Small RNAs have been shown to localize to many special subcellular organelles, including membrane compartments (mitochondria, secreted exosomes and the endoplasmic reticulum) and membraneless compartments (stress granules, processing bodies and germ granules) (Jie et al., 2021; Liao et al., 2021; Phillips and Updike, 2022; Saikia et al., 2023; Zhou et al., 2017). Small RNAs play vital roles in the maintenance of organelle homeostasis. Dysfunction of small RNAs leads to various diseases, such as neurodegenerative diseases and cancer (Barrière and Bertrand, 2022; Hombach and Kretz, 2016).

Here, using CRISPR/Cas9 technology, we generated a GFP-tagged NRDE-3 knock-in transgene. NRDE-3 was expressed in oocytes, early and late embryos, and somatic cells and was enriched in the nucleus. Strikingly, we observed that NRDE-3 could also accumulate in the peri-centrosomal foci in a manner dependent on its PAZ domain and RdRPs. Therefore, our findings suggest that the peri-centrosomal region may also be a platform for RNAi-mediated gene regulation.

RESULTS

NRDE-3 is widely expressed in germlines, oocytes, early and late embryos and soma

NRDE-3 is a nuclear Argonaute protein and is required for the nuclear RNAi pathway. Previous work constructed a low-copy green fluorescent protein (GFP) and full-length NRDE-3 fusion transgene driven by the *nrde-3* promoter through a microparticle-mediated bombardment method (Figure 1A) (Guang et al., 2008), which contained approximately 11 copies of the 3xFLAG::GFP::NRDE-3 fusion gene in the genome (Figure S1A). The multi-copy NRDE-3 transgene caused the Eri phenotype and enhanced feeding RNAi response (Zhuang et al., 2013). Here, we used CRISPR/Cas9 gene editing technology to knock in a 3xFLAG::GFP tag onto the N-terminus of the endogenous gene locus of NRDE-3 (Figure 1A) and confirmed its copy number via real-time PCR (Figure S1A).

To confirm the function of the *in situ* tagged NRDE-3, we tested its ability to silence nuclear-localized RNAs. *lir-1* and *lin-26* are co-transcribed in an operon, and the loss of *lir-1* is viable, whereas the loss of *lin-26* results in larval lethality. RNAi targeting *lir-1* also caused larval lethality via nuclear RNAi machinery-mediated gene silencing of the nucleus-localized *lir-1–lin-26* polycistronic RNA (Bosher et al., 1999; Guang et al., 2008; Lewis et al., 2020). The response of 3xFLAG::GFP::NRDE-3(ust574, KI) animals to *lir-1* RNAi was similar to that of wild-type N2 animals (Figure S1B). In addition, *dpy-11* RNAi caused nuclear RNAi-dependent gene silencing in both the P0 and F_1 generations (Zhuang et al., 2013). Single-copy 3xFLAG::GFP::NRDE-3 (ust574, KI) transgenic animals exhibited a similar response to RNAi to that of wild-type N2 animals upon *dpy-11* RNAi (Figure S1C). Therefore, the 3xFLAG::GFP::NRDE-3 (ust574, KI) transgene largely recapitulated the endogenous functions of NRDE-3 without causing an extra Eri phenotype, as did the multicopy 3xFLAG::GFP::NRDE-3 (ggIS1, bombardment) transgene (Figure S1A–C) (Zhuang et al., 2013). For simplicity, the 3xFLAG::GFP::NRDE-3 (ust574, KI) transgene is abbreviated as GFP::NRDE-3 until otherwise specified in the text.

GFP::NRDE-3 was expressed in germline, oocyte, early and late embryos and larval soma (Figure 1B–D; Figure S1D and E), which is consistent with recent research from other laboratories (Liu et al., 2023; Seroussi et al., 2023).

We investigated NRDE-3-associated siRNAs in embryos. NRDE-3 was immunoprecipitated from the embryo lysates and the associated small RNAs were subjected to deep sequencing via a 5′-end phosphate-independent method (Guang et al., 2008; Zhou et al., 2014). The NRDE-3-associated embryo-specific siRNAs were 22 nt in length, and the majority of them started with G at their 5′ ends, which is consistent with the properties of 22G RNAs (Figure S2A). Approximately 79% of NRDE-3-associated 22G RNAs target protein-coding genes. We selected potential NRDE-3-specific targets that had more than 25 reads per million small RNAs and identified 602 NRDE-3 target genes. The ectopically expressed 3xFLAG::GFP::NRDE-3 (ggIS1, bombardment)-associated siRNA targets were largely a subset of the 3xFLAG::GFP::NRDE-3 (ust574, KI) targets (Figure S2B), which is consistent with the expression stage of both GFP::NRDE-3 strains in embryos.

The embryo-specific NRDE-3 targets exhibited extensive overlap with those of HRDE-1 (Figure S2C), the other germline-expressed nuclear Argonaute protein (Xu et al., 2018). The NRDE-3 embryo-specific targets also showed strong overlap with *glp-4*-dependent genes (Figure S2D) (Xu et al., 2018), suggesting that NRDE-3-associated siRNAs may target germline-enriched genes. The WAGO-1 and WAGO-4 targets exhibited modest overlap with the NRDE-3 targets (Figure S2E and F). However, CSR-1 targets exhibited only a slight overlap with NRDE-3 targets (Xu et al., 2018) (Figure S2G).

Overall, NRDE-3 was expressed in the germline, oocytes, early and late embryos, and larval somatic cells.

The nuclear localization of NRDE-3 depends on RNA-dependent RNA polymerases

Previous work has shown that NRDE-3 is localized to the nucleus or nucleolus in somatic cells, depending on the presence of 22G RNAs (Guang et al., 2008). Consistent with these findings, mutations in *eri-1* and *ergo-1*, which are required for the biogenesis of endogenous siRNAs (Guang et al., 2008), decreased the nuclear localization of NRDE-3 in the soma, as shown by both

https://doi.org/10.1007/s11427-024-2818-7

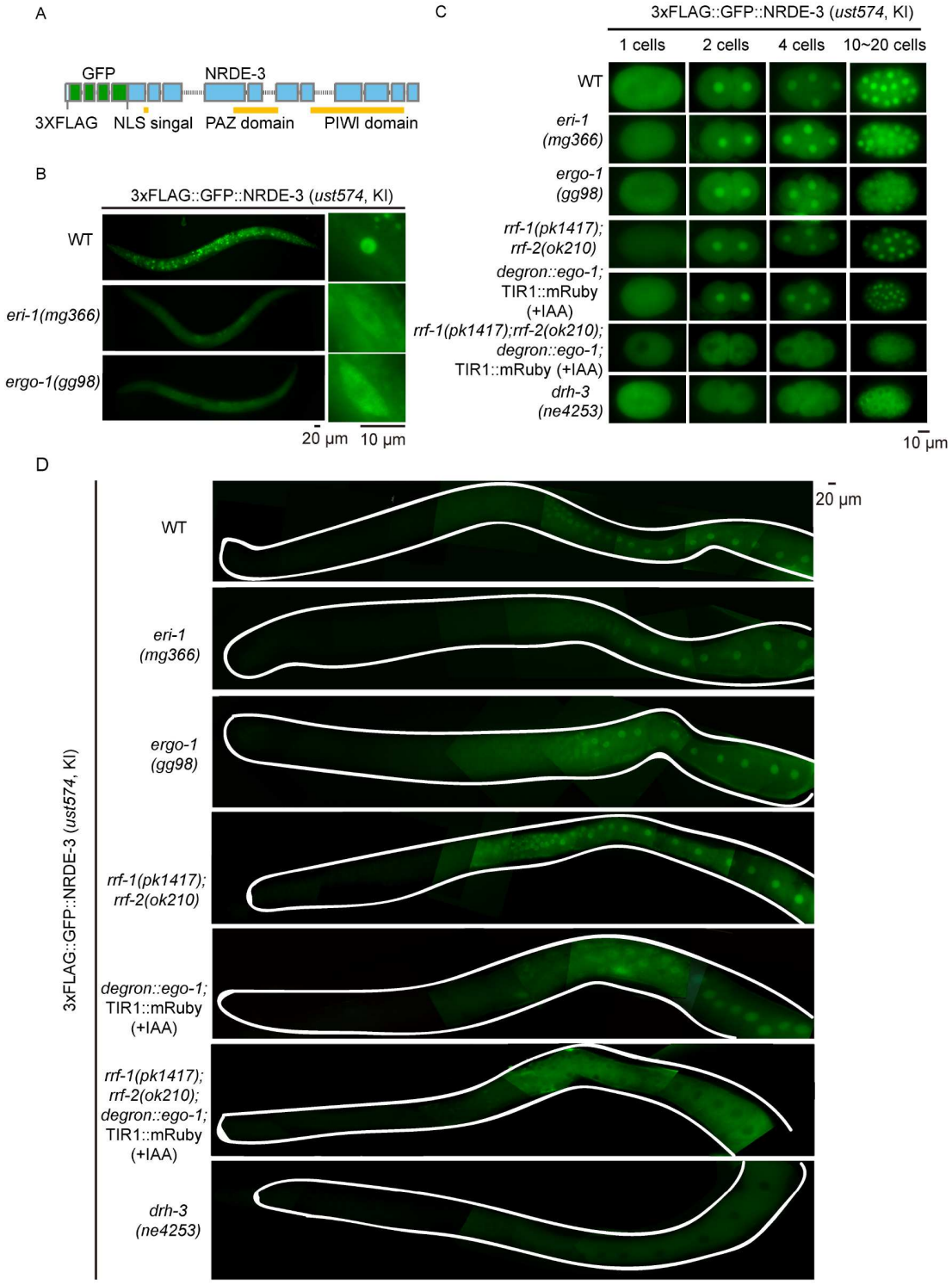

Figure 1. NRDE-3 is widely expressed in germlines, oocytes, early and late embryos and somatic cells. A, Schematic of NRDE-3 and the 3xFLAG::GFP tag. NLS, nuclear localization signal. B, Fluorescence microscopy images of 3xFLAG::GFP::NRDE-3(ust574, KI) in L4 stage animals (left) and seam cells (right) of the indicated genotypes. C, Fluorescence microscopy images of 3xFLAG::GFP::NRDE-3 (ust574, KI) in embryonic stages in the indicated background. For *degron::ego-1* animals, synchronized embryos were grown on NGM plates seeded with OP50 supplemented with 1 mmol L^{-1} IAA. For the *rrf-1*;*rrf-2*;*degron::ego-1* animals, synchronized animals were grown on OP50 plates and shifted to NGM plates containing 1 mmol L^{-1} IAA at the L4 stage. Pictures were taken 48 h after IAA treatment. D, Fluorescence microscopy images of the dissected gravid adult germline.

3xFLAG::GFP::NRDE-3 (ggIS1, bombardment) (Guang et al., 2008; Lee et al., 2006) and 3xFLAG::GFP::NRDE-3 (ust574, KI) (Figure 1B).

Interestingly, mutations in *eri-1* and *ergo-1* did not significantly deplete the nuclear accumulation of NRDE-3 in the germline, oocytes or early embryos. NRDE-3 remained in the

nucleus in the mutants (Figure 1C and D), suggesting that NRDE-3 may bind alternative cohorts of siRNAs in cells even when *eri-1*- and *ergo-1*-dependent siRNAs are depleted. The *C. elegans* genome encodes four RNA-dependent RNA polymerases, namely, RRF-1, RRF-2, RRF-3 and EGO-1 (Sijen et al., 2001; Smardon et al., 2000). Among them, RRF-1 localizes to Mutator foci, where it synthesizes WAGO class 22G RNAs using pUGylated RNA fragments as templates (Phillips et al., 2012). EGO-1 is a germline-specific RdRP that is essential for viability and synthesizes CSR-1 class 22G RNAs in E granules (Billi et al., 2014; Shukla et al., 2020). We generated a *degron::ego-1* strain by the CRISPR/Cas9 method to degrade EGO-1 proteins upon treatment with IAA (Zhang et al., 2015). The function of RRF-2 remains unclear.

In both the *rrf-1*;*rrf-2* double mutant and the *degron::ego-1* (+*IAA*) mutant, NRDE-3 was enriched in the nucleus in the germline, oocytes and early embryos (Figure 1C and D). However, in the *rrf-1*;*rrf-2*;*degron::ego-1* (+*IAA*) triple mutant, NRDE-3 accumulated in the cytoplasm in the germline, oocytes and early embryos at 20°C (Figure 1C and D). DRH-3 interacts with EGO-1, is enriched in both the E-granule and mutator foci and is required for both RRF-1- and EGO-1-dependent 22G RNA biogenesis (Chen et al., 2024). In the *drh-3* mutant, NRDE-3 accumulates in the cytoplasm. The depletion of NRDE-3 from the nucleus in the *rrf-1*;*rrf-2*;*degron::ego-1* (+*IAA*) triple mutant and in the *drh-3* mutant suggested that NRDE-3 associated with 22G RNAs generated by both RRF-1- and EGO-1-dependent production machineries.

NRDE-3 accumulated in the perinuclear foci in embryos

Interestingly, although *eri-1* and *ergo-1* mutation did not abolish the nuclear accumulation of NRDE-3 in the germline and early embryos, we noticed that GFP::NRDE-3 was able to accumulate to the distinct perinuclear foci in embryos in *eri-1*(–) and *ergo-1* (–) animals (Figure 2A and B). In *drh-3* mutant, although NRDE-3 was depleted from the nucleus and accumulated in the cytoplasm (Figure 1C and D), we also observed the perinuclear foci-accumulation of NRDE-3 in embryos (Figure 2A and B). However, no perinuclear foci accumulation of NRDE-3 were identified in any of the three mutant background: *degron::ego-1* (+*IAA*), *rrf-1*;*rrf-2* double mutant; *rrf-1*;*rrf-2*;*degron::ego-1*(+*IAA*) triple mutant.

To facilitate fluorescence detection of the perinuclear foci-enriched NRDE-3, we generated a much brighter GFP-NRDE-3 transgene using the *mex-5* promoter. The *mex-5* promoter-driven single-copy *mex-5p::3xFLAG::GFP::NRDE-3* transgene was inserted into the ttTi5605 site on chromosome II via CRISPR/Cas9 method. Similarly, the *mex-5* promoter-driven GFP::NRDE-3 was strongly enriched in the perinuclear foci in *drh-3* background (Figure 2C and D).

The nuclear localization of NRDE-3 requires its ability to bind 22G RNAs (Guang et al., 2008). We tested whether the perinuclear foci-accumulation of NRDE-3 also requires the presence of siRNA binding. PAZ domain is required for Arognaute proteins, including NRDE-3, to bind small RNAs (Guang et al., 2008). We genearated a *mex-5p::3xFLAG::GFP::NRDE-3*(**PAZ, Y463A, Y464A*) mutant transgene (Figure S3A). Consistent with previous reports (Guang et al., 2008), *NRDE-3* (**PAZ, Y463A, Y464A*) protein accumulated in the cytoplasm as well. Notably, we did not observe the perinuclear foci accumulation of GFP::NRDE-3(*PAZ) in *drh-3* mutant, suggesting that small RNA binding is essential for NRDE-3 to enrich in the perinuclear foci (Figure 2C and D).

The nuclear localization signal (NLS) sequence is important for NRDE-3 to translocate to the nucleus upon binding to siRNAs (Guang et al., 2008). The mutation in NLS(K80A, R81A, K82A) in NRDE-3 abrogated the nuclear accumulation of NRDE-3 and prohibited its ability to rescue nuclear RNAi defects in *nrde-3* animals (Guang et al., 2008). We generated *mex-5p::GFP::NRDE-3*(**NLS, K80A, R81A, K82A, KI*) transgenic animals (Figure S3A) and observed the depletion from the nucleus in both wild-type N2 background and *drh-3* mutant embryos. Strikingly, in wild-type N2 background, approximately 11% early embryos revealed the perinuclear foci accumulation of NRDE-3(*NLS). In addition, the percentage increased to approximately 100% in *drh-3* mutants (Figure 2C and D).

In the nucleus, siRNAs guide NRDE-3 to targeted pre-mRNAs and further recruit NRDE-2 to induce epigenetic modifications and gene silencing (Guang et al., 2010). However, we did not observe the perinuclear foci accumulation of NRDE-2 in both wild-type N2 background and *drh-3* mutant animals (Figure S3B), suggesting that NRDE-3 may target the nucleic acids in the perinuclear foci independent of other downstream NRDE factors.

We also tested whether other germline Argonaute proteins could accumulate in the perinuclear foci in embryos. However, neither HRDE-1 nor WAGO-4 showed the perinuclear foci accumulation in both wild-type N2 background and *drh-3* mutant animals (Figure S3C).

We tested various environmental conditions including culturing at 4°C, 15°C, 25°C or 37°C, starvation, and treatment with actinomycin D, yet did not observe perinuclear focus formation in 3xFLAG::GFP::NRDE-3 (*ust574*, KI) and *mex-5p::*GFP::NRDE-3 animals (Figure S4A–D).

To further confirm that the presence of 22G siRNAs contributes to the perinuclear foci accumulation of NRDE-3, we investigated the NRDE-3 foci in RdRP mutant animals. We introduced *rrf-1*;*rrf-2*;*degron::ego-1*(+*IAA*) into *eri-1*(–) animals (Figure 2D). The mutation of RRF-1, RRF-2 and EGO-1 together may deplete most, if not all, of the endogenous 22G RNAs (Billi et al., 2014). In the *rrf-1*;*rrf-2* double mutant, NRDE-3 still accumulated to distinct perinuclear foci in *eri-1*(–) animals (Figure 2D and E). However, in *rrf-1*;*rrf-2*;*degron::ego-1*(+*IAA*) triple mutant, the perinuclear foci accumulation of NRDE-3 was drastically reduced. Interestingly, the perinuclear foci accumulation of NRDE-3 is temperature sensitive. Growing animals at 25°C for 12 h could deplete the perinuclear foci-enriched NRDE-3 (Figure S5A–D).

Therefore, NRDE-3 could accumulate in distinct perinuclear foci in embryos, which depends on the binding of siRNAs.

NRDE-3 accumulates in peri-centrosomal foci

We noticed that NRDE-3 accumulated in either one perinuclear focus or two perinuclear foci which were on the opposite side of the nucleus, in *eri-1*, *ergo-1* and *drh-3* animals. Therefore, we suspected that the focus is the centrosome or at least in peri-centrosomal region. To test this idea, we generated a number of tagRFP- and mCherry-tagged centriole proteins and pericentriolar material (PCM) and examined their relative subcellular localization with GFP::NRDE-3.

SAS-4, SAS-5 and SAS-6 are components of the centriole. AIR-

https://doi.org/10.1007/s11427-024-2818-7

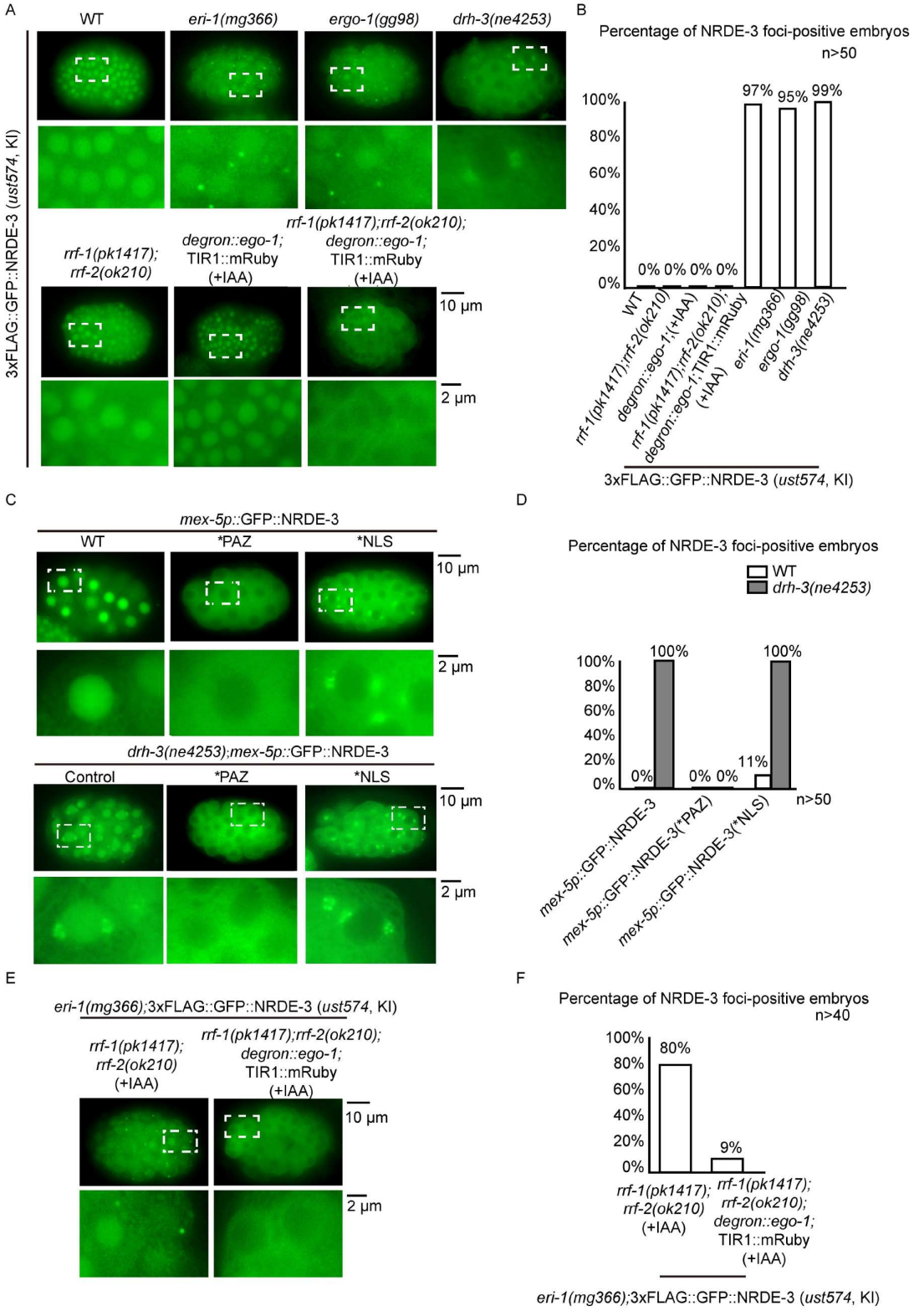

Figure 2. NRDE-3 accumulates in the perinuclear foci in embryos. A, Fluorescence microscopy images of 3xFLAG::GFP::NRDE-3(ust574, KI) in late embryos in the indicated genotypes. B, The bar graph displays the percentage of NRDE-3 foci-positive embryos. An embryo was defined as positive if one or more NRDE-3 foci were observed. At least 50 embryos were imaged for each genotype. C, Fluorescence microscopy images of *mex*-5 promoter-driven GFP::NRDE-3, GFP::NRDE-3(*PAZ) and GFP::NRDE-3(*NLS) in embryonic stages in indicated background. *PAZ, (Y463A, Y464A); *NLS, (K80A, R81A, K82A). D, The bar graph displays the percentage of NRDE-3 foci-positive embryos. An embryo was defined as positive if one or more NRDE-3 foci were observed. At least 50 embryos were imaged for each genotype. E, Fluorescence microscopy images of *eri-1*(*mg366*); 3xFLAG::GFP::NRDE-3(ust574, KI) in embryos of the indicated genotypes. In *rrf-1*;*rrf-2* background, synchronized embryos were grown on NGM plates seeded with OP50 and 1 mmol L^{-1} IAA. For *rrf-1*;*rrf-2*;*degron::ego-1* animals, synchronized animals were grown on OP50 and at L4 stage shifted to NGM plates containing 1 mmol L^{-1} IAA. Pictures were taken 48 h later after IAA treatment. F, The bar graph displays the percentage of NRDE-3 foci-positive embryos. At least 40 embryos were imaged for each genotype.

1 is a component of the pericentriolar material. γ-Tubulin is a core component of the centrosome and serves as the nucleation center for the polymerization of α/β-tubulin dimers into microtubules and the organization of centrosomal microtubule asters (Bobinnec et al., 2000; Hurd, 2018; Strome et al., 2001). In *eri-1*, *ergo-1* and *drh-3* mutants, GFP::NRDE-3 consistently accumulated in foci neighboring to the γ-tubulin, AIR-1, SAS-4, SAS-5 and SAS-6-marked centrosome (Figures 3A; Figure S6A and B).

tbb-2 encodes a β-tubulin in *C. elegans*, which contributes to spindle assembly and microtubule formation during mitosis and meiosis. TBB-2 is an essential component of the centrosome center-centriole, and also a component of the centrosome-based spindle in the early embryos (Pintard and Bowerman, 2019). We generated single-copy *mex-5* promoter-driven tagRFP-tagged TBB-2 transgenic strains (termed tagRPF::TBB-2). NRDE-3 foci also neighbor the microtubule marker TBB-2 (Figure 3B). TBB-2 was chosen as a marker for better simultaneous visualizing of GFP::NRDE-3 localization.

Although shifting animals to 25°C could deplete the peri-centrosomal foci-enriched NRDE-3, the temperature change did not significantly alter the TBB-2-marked centrosome (Figure S7A). Therefore, we concluded that NRDE-3 may accumulate in the peri-centrosomal foci.

CSR-1 is the only Argonaute protein essential for fertility and forms diverse granules in embryos (Seroussi et al., 2023), yet we failed to detect the colocalization of CSR-1 with γ-tubulin and AIR-1-marked PCM (Figure S7B).

NRDE-3 accumulates in the peri-centrosomal foci and spindle during the cell cycle

The centrosome is highly dynamic and required for faithful cell division during the cell cycle (Pintard and Bowerman, 2019). To investigate whether NRDE-3 also accumulates in centrosome in a cell cycle-dependent manner during embryogenesis, we used tagRFP::TBB-2 as centrosome marker and BFP::H2B as chromatin marker and quantified the proportion of NRDE-3 foci at different cell cycle phases. NRDE-3 was significantly enriched at the peri-centrosomal region throughout all mitotic phases (Figures 4A–D). However, the NRDE-3(*PAZ) mutant did not exhibit centrosome and spindle enrichment, suggesting that siRNA binding is essential for NRDE-3 to accumulate in the peri-centrosomal region and spindle structure (Figure S8A and B). The NRDE-3(*NLS) also revealed enrichment in the peri-centrosomal region and spindle during the cell cycle in wild-type N2 background animals. The mutation in *drh-3* strongly enhanced the centrosome and spindle accumulation of NRDE-3 (*NLS) (Figure S9A and B). Notably, during cell division, NRDE-3 localized near the spindle during early embryogenesis. We observed that NRDE-3 likely localizes to the microtubule-organizing center (MTOC), polar microtubules, and kinetochore microtubules (K-fibers) during metaphase (Figures 4C; Figure S9C). Therefore, we conclude that NRDE-3 could accumulate in the peri-centrosomal region and spindle during the cell cycle, which depends on the binding of siRNAs.

Identification of peri-centrosome-enriched siRNAs in *C. elegans*

The small size of the centrosome and the embryonic shell hindered us from biochemically purifying centrosomes in *C. elegans*. Meanwhile, because of the size of nucleus is much larger than the size of pericentrosomal NRDE-3 foci, it is very likely that pericentrosmal NRDE-3 may only account for a small portion of cellular NRDE-3 protein pools, similar does pericentrosmal NRDE-3-associated siRNAs. To specifically identify peri-centrosome-enriched siRNAs, we compared NRDE-3(*NLS)- and TBB-2-associated siRNAs in *drh-3* mutant animals versus in wild-type animals, focusing on upregulated siRNAs, as the *drh-3* mutation significantly increased peri-centrosomal accumulation of NRDE-3 (Figure 5A).

We immunoprecipitated NRDE-3 from NRDE-3(*NLS) strain and TBB-2 from tagRFP::TBB-2; NRDE-3(*NLS) strain at embryonic stage in both *drh-3*(+) and *drh-3*(–) animals. The associated siRNAs were isolated and subjected to deep sequencing in a 5′-end phosphate-independent manner. Approximately 90% of NRDE-3(*NLS)-associated small RNAs targeted protein-coding genes in both wild-type background and *drh-3* animals. For TBB-2-immunoprecipitated small RNAs, the vast majority were miRNAs and siRNAs which target protein-coding genes. The siRNAs which were upregulated in NRDE-3(*NLS) (*drh-3*(–) vs wild type) and TBB-2 (*drh-3*(–) vs wild type) background were subsequently compared and 489 shared siRNAs were identified, which were potentially peri-centrosome-enriched siRNAs (Figure 5B, Table S1). These peri-centrosome-enriched siRNAs revealed a large overlap with HERD-1, CSR-1 and WAGO-4 targets and *glp-4*-dependent targets, but minimal overlap with WAGO-1 targets (Figure 5C).

The 22G RNAs generated by EGO-1 have been classed to E-class siRNAs(Chen et al., 2024). Then, E-class siRNAs were further classified to E-class 5′ siRNAs and E-class 3′ siRNAs, which predominantly mapped to the 5′ portion of the E-class genes and 3′ end, respectively. The siRNAs targeting the 3′ most of the E-class genes relied on EGO-1 and typically include the last exon of the E-class genes (Chen et al., 2024). Metagene analysis revealed that the peri-centrosome-enriched siRNAs predominantly mapped to the 3′ portion of the target genes (Figure 5D).

A number of mRNAs have been reported to localize in centrosomes in human cells, *Drosophila* and *C. elegans* (Safieddine et al., 2021). Three of the genes, *aspm-1*, *mesp-1* and *lin-5*, were identified among the top candidates in the overlap 489 target gene set, revealed abundant siRNA reads and increased siRNA association in *drh-3*(–) mutant vs *drh-3*(+) animals (Figure 5E). *aspm-1* mRNA was reported to be enriched on mitotic centrosomes across all phases of cell division in *Drosophila* to human cells (Ryder and Lerit, 2018; Safieddine et al., 2021; Sepulveda et al., 2018). Although *mesp-1* mRNA has not been reported to be enriched in the centrosome, MESP-1 functions to sort microtubules of mixed polarity into a configuration in which the minus ends are away from the chromosomes, enabling the formation of nascent poles (Wolff et al., 2016). LIN-5 protein binds the dynein complex, localizes in the spindle and involves in microtubule cytoskeleton organization (Lorson et al., 2000). *lin-5* mRNA was previously shown to be enriched in centrosomes by FISH assay. We noticed the increase of siRNAs targeting the 3′ portion of the *aspm-1*, *mesp-1* and *lin-5* genes (Figure 5E) as well as in other peri-centrosomal targets (Figure S10), as shown by IGV.

The integrity of the centrosome is required for the peri-centrosomal accumulation of NRDE-3

We then tested whether the peri-centrosomal accumulation of

https://doi.org/10.1007/s11427-024-2818-7

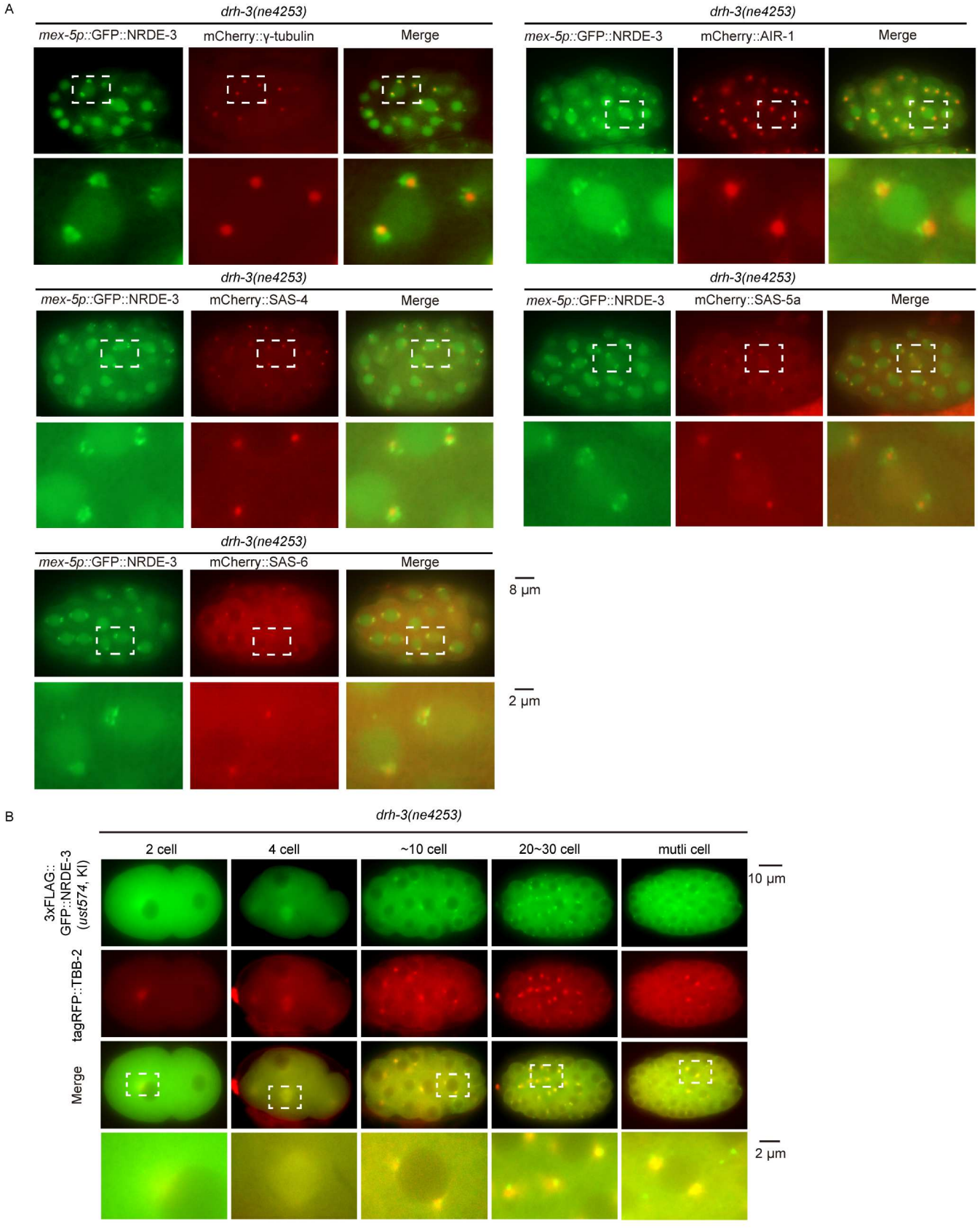

Figure 3. NRDE-3 accumulates in the peri-centrosomal foci. A, Images of *mex-5p*::GFP::NRDE-3 with indicated mCherry-tagged centrosome proteins in *drh-3*(*ne4253*) background. B, Images of 3xFLAG::GFP::NRDE-3(ust574, KI) with tagRFP::TBB-2 in embryos in *drh-3*(*ne4253*) background.

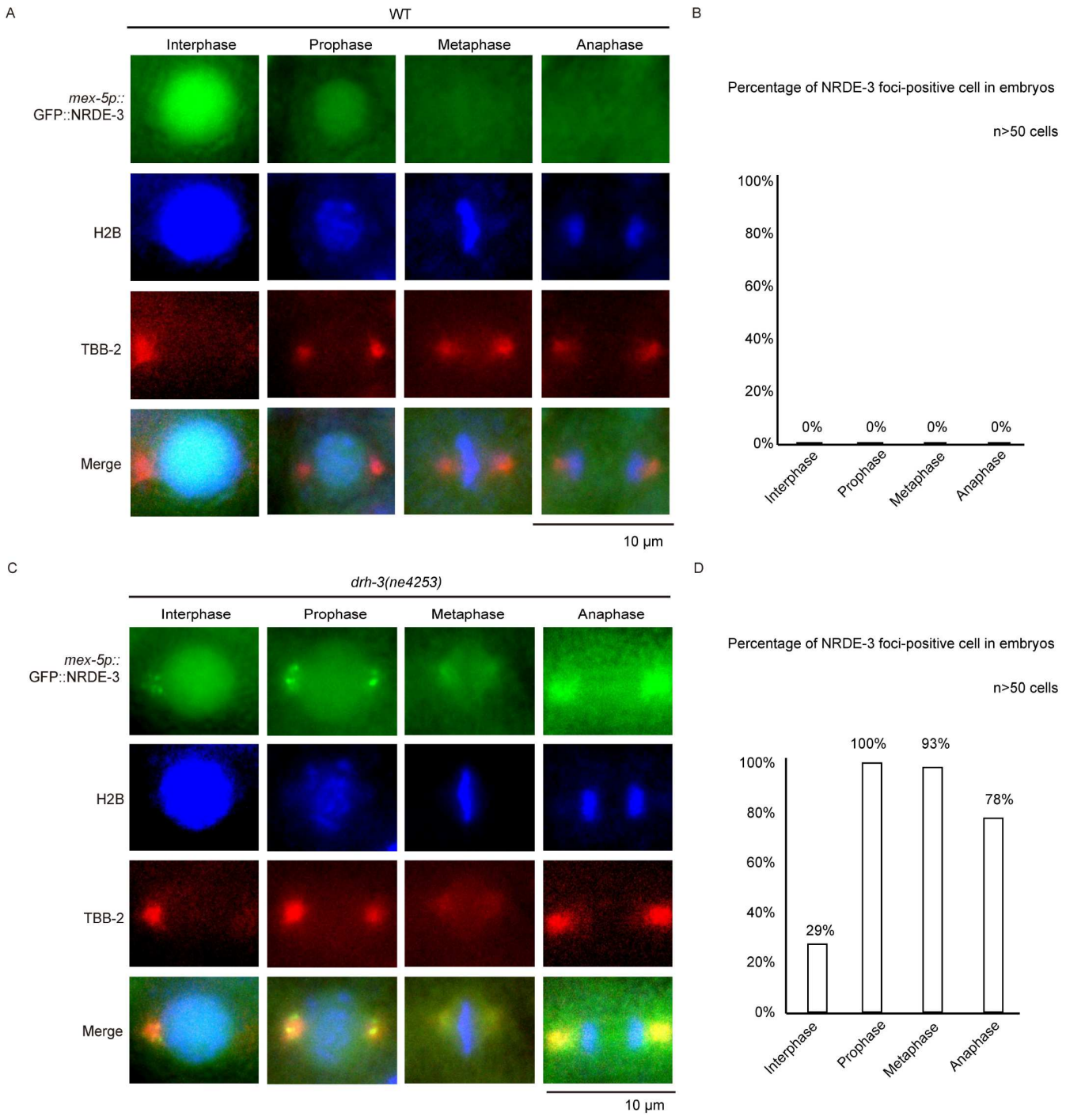

Figure 4. NRDE-3 accumulates in the peri-centrosomal foci and spindle during the cell cycle. A and C, Fluorescence microscopy images of indicated animals in interphase and mitosis. B and D, Bar graph depicting the percentage of peri-centrosomal localization of NRDE-3 foci in cells in each phase. Embryos at 10–30 cell stage were selected for quantification. For each embryo, each cell was assigned to different mitosis phases using BFP::H2B as a marker. We defined that one or more NRDE-3 foci in one cell as positive and then counted the percentage of positive cells in each phase, at least 50 cells were quantified for each phase.

NRDE-3 relies on the integrity of centriole proteins and pericentriolar material (PCM). In *eri-1*(*mg366*) and *ergo-1* (*gg98*) background, GFP::NRDE-3 animals were fed by bacteria expressing dsRNAs targeting centriole, pericentriolar material, and their interactors. Synchronized embryos were hatched and cultured on NGM plates for 41 h. L4 animals were then transferred to RNAi plates and F_1 embryos were examined.

In F_1 embryos, knocking down both PCM components and centriole proteins not only abolished the centrosome structure, as shown by tagRFP::AIR-1 and tagRFP::SAS-4 markers but also depleted the foci localization of GFP::NRDE-3 (Figure 6A–D; Figure S11), suggesting that centrosome integrity is essential for

https://doi.org/10.1007/s11427-024-2818-7

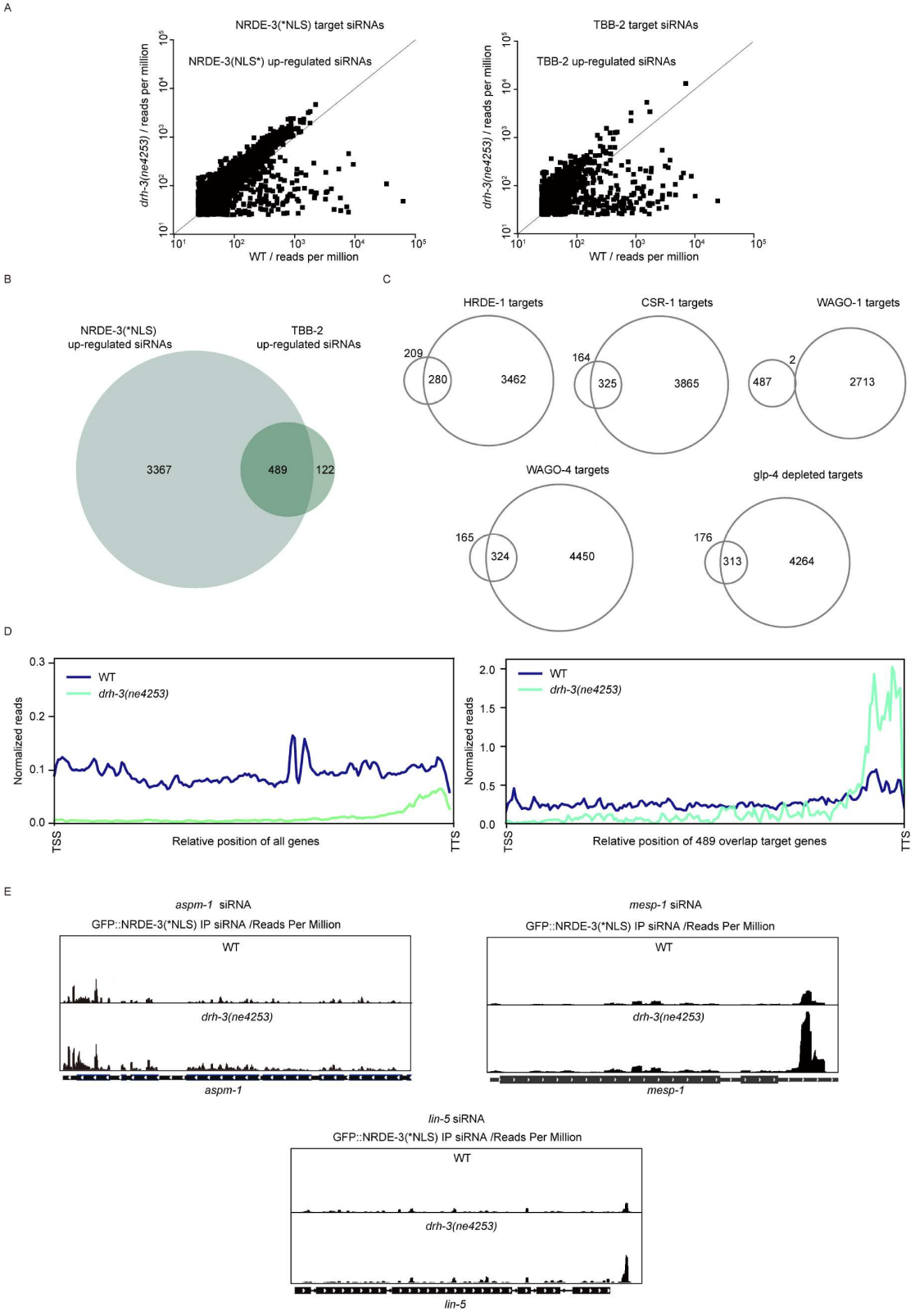

Figure 5. Identification of peri-centrosome-enriched siRNAs in *C. elegans*. A, Scatterplots showing gene-by-gene comparisons of NRDE-3(*NLS)- and TBB-2- associated small RNA reads between *drh-3*(*ne4253*) and wild-type animals. Each dot represents a gene. Cutoff>25 reads per million. B, Venn diagrams showing the overlap between upregulated siRNAs in the gene sets of NRDE-3(*NLS) (*drh-3*(–) vs wild type) and TBB-2 (*drh-3*(–) vs wild type). *drh-3*(*ne4253*)/wild type fold change>1.3. The overlap is annotated as potentially peri-centrosome-enriched siRNAs. C, Venn diagrams showing comparisons between the 489 overlap siRNAs and other known siRNA categories. D, Metaprofile analysis showing the distribution of normalized 22G RNA reads (RPM) along all genes (left) and the 489 overlap siRNAs (right) in the indicated animals. E, The distribution of normalized NRDE-3(*NLS)-associated small RNA reads across *aspm-1*, *mesp-1* and *lin-5* genomic loci in wild type and *drh-3*(*ne4253*) animals.

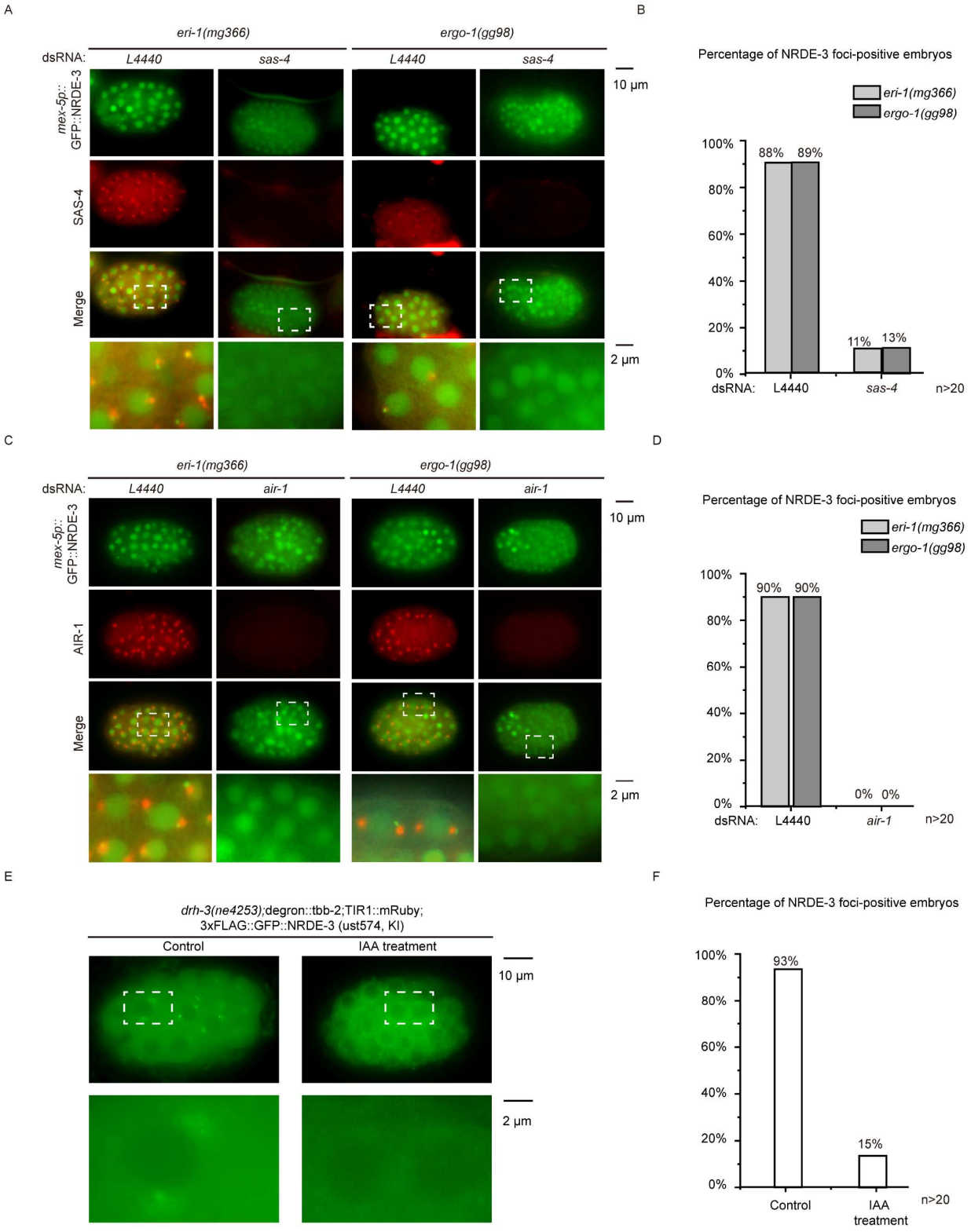

Figure 6. The integrity of the centrosome is required for the peri-centrosomal accumulation of NRDE-3. A, Images of *eri-1*(–); GFP::NRDE-3; mCherry::SAS-4 (left) and *ergo-1*(–); GFP::NRDE-3; mCherry::SAS-4 (right) animals after *sas-4* RNAi. Synchronized embryos were hatched and cultured on NGM plates for 41 h and then at L4 animals were transferred to RNAi plates and F_1 embryos were imaged. B, The bar graph displays the percentage of NRDE-3 foci-positive embryos. An embryo was defined as positive if one or more NRDE-3 foci were observed. At least 20 embryos were imaged for each RNAi experiment. C, Images of indicated animals after *air-1* RNAi. D, The bar graph displays the percentage of NRDE-3 foci-positive embryos. E, Fluorescence microscopy images of *drh-3*(*ne4253*); *degron*::tbb-2; TIR1::mRuby; 3xFLAG::GFP::NRDE-3 (ust574, KI) in embryos. Synchronized embryos were grown on NGM plates seeded with OP50 and 1 mmol L^{-1} IAA. Pictures were taken 48 h later after IAA treatment. F, The bar graph displays the percentage of NRDE-3 foci-positive embryos.

https://doi.org/10.1007/s11427-024-2818-7

the NRDE-3 accumulation in the peri-centrosomal foci.

Since the *drh-3*(*ne4253*) mutant is defective in feeding RNAi experiments, we generated a *degron::tbb-2* strain via the CRISPR/Cas9 method to degrade TBB-2 proteins upon treatment with IAA. In *drh-3*(–) background animals, knocking down TBB-2 also depleted the peri-centrosomal foci localization of GFP::NRDE-3 (Figure 6E and F).

Peri-centrosomal accumulation of NRDE-3 is important for development of *C. elegans*.

To test the importance of peri-centrosomal NRDE-3 localization, we compared the brood size, hatch rate and developmental progress of *nrde-3* mutants in both wild-type N2 and *drh-3* (*ne4253*) backgrounds. The introduction of *nrde-3*(*gg66*) mutation results in a modest reduction in brood size in both wild-type and *drh-3* background (Figure 7A). The embryo hatch rate of the *drh-3*; *nrde-3* double mutant is significantly lower than that of the *drh-3* single mutant (Figure 7B). In addition, *nrde-3*(*gg66*) mutants exhibited a slower growth rate than control animals (Figure 7C).

Therefore, we concluded that the peri-centrosomal localization of NRDE-3 may play important roles in both fertility and development in *C. elegans*.

DISCUSSION

Taken together, the results of this study revealed that the nuclear Argonaute protein NRDE-3 is expressed in the germline, oocytes, early and late embryos, and larval soma. Specifically, NRDE-3 can accumulate in the peri-centrosomal foci through a process dependent on its ability to bind siRNA and the integrity of centriole proteins and pericentriolar material (PCM) components, especially in *eri-1*, *ergo-1*, and *drh-3* background (Figure 7D), which implies that the pericentrosomal region may also be a platform for RNAi-mediated gene regulation. Moreover, this work suggested that the subcellular localization of NRDE-3 may be used to track the dynamics and transport of RNAs in distinct subcellular organelles.

The mechanism of NRDE-3's peri-centrosomal accumulation

Several lines of evidence support that siRNA sequences direct NRDE-3 to the peri-centrosomal foci. First, the NRDE-3(*PAZ) mutant, which abolishes its siRNA binding ability, could not accumulate in peri-centrosomal foci (Figure 2C and D). Second, in the RdRP mutant, which is defective in the production of certain class of endo-siRNAs, the number of peri-centrosomal NRDE-3 foci is significantly reduced as well (Figure 2E and F). Third, centrosomal or peri-centrosomal regions indeed contain mRNAs, which have been reported in several organisms including *C. elegans* (Alliegro and Alliegro, 2008; Alliegro et al., 2006; Bergalet et al., 2020; Blower et al., 2007; Lambert and Nagy, 2002; Lécuyer et al., 2007; Raff et al., 1990; Sepulveda et al., 2018).

Our previous work showed that E-class siRNAs are categorized into E-class 5′ siRNAs and E-class 3′ siRNAs, which predominantly map to the 5′ and 3′ regions of E-class genes, respectively (Chen et al., 2024). In the *drh-3* mutant, we observed that, although the E-class 5′ siRNAs were depleted, the E-class 3′ siRNAs were increased in a cohort of 489 overlapped target genes (Figure 5D and E), which may direct NRDE-3 to the peri-centrosome-localized mRNA targets. Moreover, previous work has shown that E-class 3′ siRNAs are likely generated by the EGO module in the cytosol (Chen et al., 2024). This work revealed that, in the *drh-3* mutant, cytoplasmic localized NRDE-3 presented more pronounced peri-centrosomal accumulation than those in *eri-1* and *ergo-1* mutants (Figure 2A). Similarly, when we ectopically expressed a mutant version of NRDE-3 with a defective NLS sequence, in which NRDE-3 is unable to translocate to the nucleus, we observed peri-centrosomal localization of NRDE-3 in approximately 11% of embryos in N2 background animals (Figure 2D).

However, peri-centrosomal NRDE-3 foci are only easily observable in certain mutant backgrounds. Further investigations are needed to determine how and why NRDE-3 could accumulate in peri-centrosomal foci under some growth or environmental conditions in wild-type animals.

The role of centrosomal siRNAs

The function of peri-centrosomal siRNAs is intriguing. Owing to technical limitations, the subcellular localization of small regulatory RNAs and their specialized functions have largely been neglected. With the development of various technologies, including the isolation of subcellular organelles and immunofluorescence localization analysis, an increasing number of studies have yielded broad insights into the subcellular localization and functions of small RNAs.

Considering that NRDE-3 is an Argonaute protein and its peri-centrosomal foci localization depends on the presence of siRNAs, we speculate that siRNAs at the peri-centrosomal region may guide Argonaute proteins to regulate gene expression at the foci.

This work revealed that the peri-centrosome-enriched siRNAs largely overlapped with CSR-1 and *glp-4*-dependent targets (Figure 5C), and predominantly mapped to the 3′ portion of the target genes (Figures 5D and E; Figure S9). We hypothesize that NRDE-3 may load a subset of CSR-1-class siRNAs in the germline to target mRNAs that are enriched in the peri-centrosomal region. Our previous work revealed that DRH-3 interacts with EGO-1 and is enriched in both the E-granule and mutator foci (Chen et al., 2024). EGO-1 accumulates in E-granule and is required for the generation of E-class 22G RNAs. CSR-1 binds a subset of the E-class siRNAs. In the *drh-3* mutant, the E-class 3′ siRNAs were increased. How and why the E-class 5′ siRNAs and E-class 3′ siRNAs are different is unclear. The peri-centrosome-enriched siRNAs show substantial overlap with CSR-1 targets (Figure 5C), hinting that peri-centrosomal NRDE-3 may regulate the same subset of germline-enriched genes as CSR-1.

In addition, the peri-centrosome-enriched siRNAs also showed considerable overlap with HRDE-1 and WAGO-4 targets (Figure 5C). Both HRDE-1 and WAGO-4 play key roles in transgenerational RNAi inheritance. Similarly, NRDE-3 has been reported to be required for intergenerational RNAi inheritance (Burton et al., 2011), consistent with its expression in the germline and early embryos.

Centrosomal RNAs (cnRNAs) have been reported to modulate centrosome homeostasis (Lerit, 2022; Ryder and Lerit, 2018; Safieddine et al., 2021). Whether NRDE-3 binds to siRNAs and regulates centrosome dynamics and cell division requires further investigation.

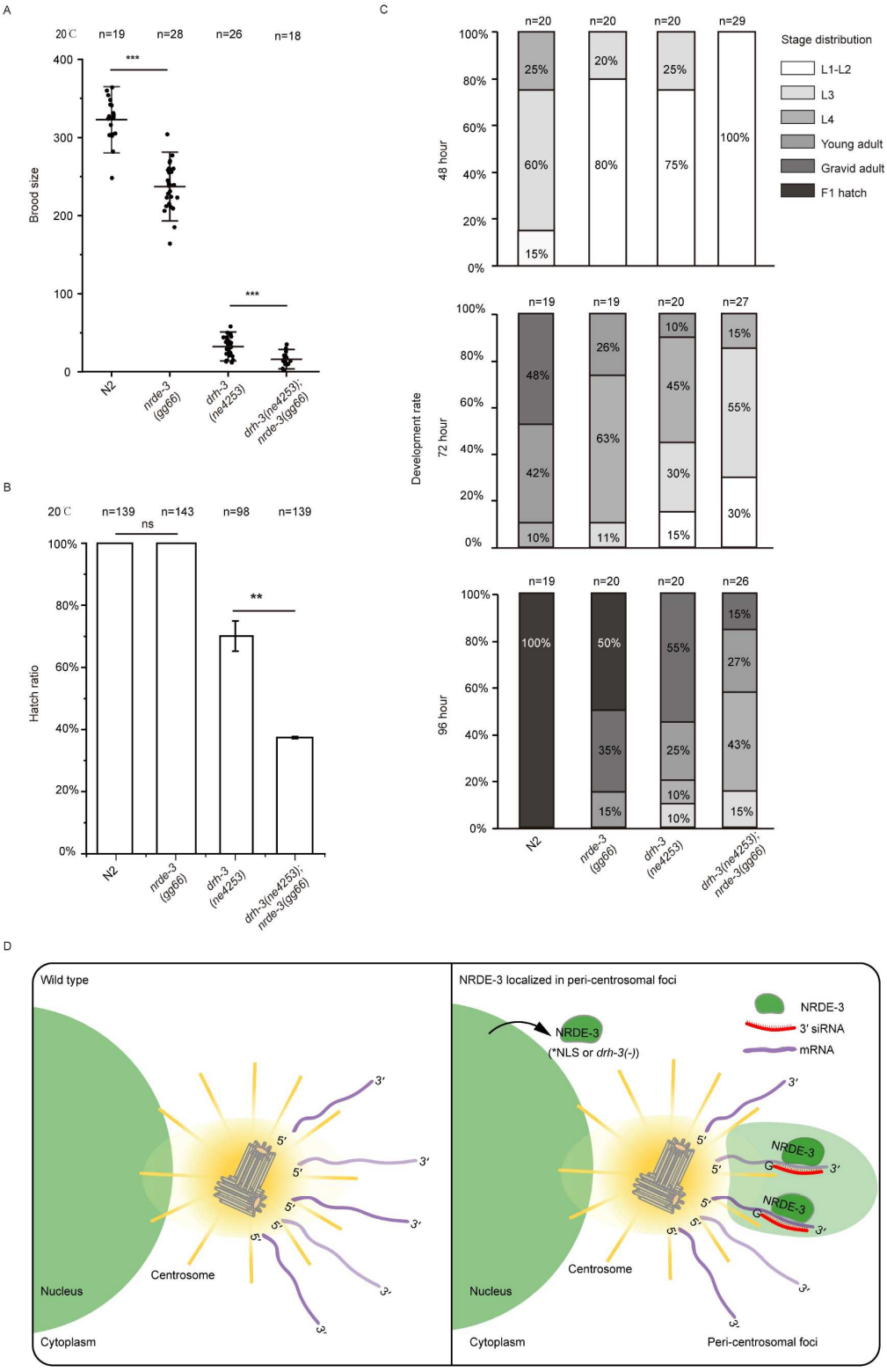

Figure 7. NRDE-3 is required for fertility and development. A, Brood size of the indicated animals at 20°C. L4 worms were transferred individually onto fresh NGM plates. The number of progeny was scored. A two-tailed *t*-test was performed to determine statistical significance. B, Hatch ratio of the indicated animals at 20°C. Synchronized adult hermaphrodites were transferred to NGM plates to lay eggs and then removed. The number of embryos and hatched larvae were recorded, and the hatch ratio was calculated as the number of hatched larvae divided by the total number of embryos. Three biological replicates were performed. C, Development rate of the indicated animals at 20°C. Synchronized adult hermaphrodites were transferred to NGM plates to lay eggs and then removed. The growth of progeny was monitored every 24 h at 20°C. D, A working model for peri-centrosomal localization of NRDE-3/siRNAs in *C. elegans*. Left: NRDE-3 localizes in nucleus in wild-type background. Right: The nuclear Argonaute protein NRDE-3 shows peri-centrosomal foci localization in *eri-1*, *ergo-1*, and *drh-3* background. NRDE-3(*NLS) can also accumulate in peri-centrosomal foci. The process depending on NRDE-3 siRNA binding ability. NRDE-3-bound 22G RNAs map to the 3′ regions of the target genes.

https://doi.org/10.1007/s11427-024-2818-7

NRDE-3 was used as a reporter to track the subcellular localization of RNAs *in vivo*

The introduction of green fluorescent protein (GFP) has revolutionized the investigation of cellular proteins *in vivo* (Shimomura, 2005; Tsien, 1998). However, although a great number of methods have been developed to assay RNAs *in vitro*, it is still difficult to directly visualize RNAs in live cells. Many methods, including FISH and fluorophore aptamer-based RNA imaging, frequently require cell fixation and are not applicable in live cells to spatiotemporally track RNAs. The MS2-MCP system has been successfully used in living organisms, yet long repetitive MS2 sequences may interfere with the normal function of RNAs. A series of small, monomeric and stable fluorescent RNAs with large Stokes shifts, including Pepper, Clivias and Okra, have been developed to enable simple and robust imaging of RNAs with minimal perturbation of the target RNA's localization and functionality (Chen et al., 2019; Huang et al., 2021; Jiang et al., 2023; Zuo et al., 2024). The development of SunTag technology has enabled the detection of cotranslational centrosomal RNA as well (Chouaib et al., 2020; Safieddine et al., 2021).

Directly visualizing the subcellular localization of siRNAs is important for many studies, including the RNAi field per se. However, given the small size of siRNAs, it is technically challenging to detect them through FISH experiments. NRDE-3 could be used to represent the subcellular localization of group of siRNAs. Alternatively, biochemical purification of cellular organelles followed by small RNA deep sequencing may help us understand the dynamics and functions of peri-centrosomal siRNAs.

Previously, centrosomes were isolated from *Spisula solidissima* oocytes and RNAs were cloned and sequenced, which were defined as centrosomal RNAs (Alliegro et al., 2006). Recently, high-throughput fluorescent *in situ* hybridization (FISH) screening and transcriptomic approaches have been applied to identify mRNAs that localize to centrosome (Lécuyer et al., 2007; Ryder et al., 2020; Safieddine et al., 2021). However, owing to the small size, it remains technically challenging to purify centrosomes from *C. elegans* embryos. Further smFISH experiments or live RNA labeling systems need to be employed to identify the peri-centrosome-localized mRNAs.

Our previous work showed that upon binding to siRNAs, NRDE-3 translocates to the nucleus and associates with targeted pre-mRNAs (Guang et al., 2010; Guang et al., 2008), or to the nucleoli and associate with pre-rRNA in the presence of risiRNAs (Liao et al., 2021; Zhou et al., 2017; Zhu et al., 2018). These results suggest that NRDE-3 could act as a siRNA transporter and enrich siRNAs in certain subcellular regions. However, it is unclear whether NRDE-3 could also be involved in transporting other size RNAs and to the peri-centrosomal region. Using smFISH or live RNA labeling method, it might be able to test whether NRDE-3 is involved in guiding mRNAs or other long RNAs to the peri-centrosomal foci. In addition, it is also very interesting to test whether the presence of peri-centrosomal foci depends on NRDE-3. Identifying another marker besides NRDE-3 will facilitate the visualization of the foci.

NRDE-3 has also been used to track transcription dynamics in live *C. elegans* (Barrière and Bertrand, 2022; Toudji-Zouaz et al., 2021). With the aid of proximity RNA labeling technology, NRDE-3 may also be used to identify the transcriptome in particular subcellular organelles.

There are some limitations in our work. The N- or C-terminal GFP tagging of tubulin can interfere with its interactions or disrupt microtubule architecture (Honda et al., 2017; Nishida et al., 2021; Xu et al., 2024). Furthermore, endogenous GFP knock-in tagging has been shown to disrupt tubulin function (Honda et al., 2017). Recent advances in AlphaFold2-guided engineering of split-GFP technology have enabled both endogenous tagging of β-tubulin without functional disruption and tissue-specific labeling of endogenous tubulins (Xu et al., 2024). Further experiments are required to understand the dynamics of peri-centrosomal NRDE-3 foci with spindle and centrosome via the newly generated functional tagged tubulin proteins.

MATERIALS AND METHODS

Strains

The Bristol strain N2 was used as the standard wild-type strain. All strains were grown at 20°C unless otherwise specified. For heat stress treatment, worms were cultured at 25°C for 12 h. The strains used in this study are listed in Supplementary Table S2.

Construction of plasmids

All plasmids were generated through the recombinational cloning of PCR-amplified fragments. A ClonExpress MultiS One Step Cloning Kit (Vazyme) was used to connect these fragments to the vector. The construction process is described in detail in the supplemental materials and methods.

Gene editing by the CRISPR/Cas9 method

For the *in situ* knock-in transgene 3xFLAG::GFP::NRDE-3 (ust574, KI), the injection mixture contained pDD162 (50 ng μL^{-1}), the NRDE-3 repair plasmid (50 ng μL^{-1}), pCFJ90 (5 ng μL^{-1}), and three sgRNAs (30 ng μL^{-1}). The mixture was injected into young adult N2 animals. The transgenes were integrated by the CRISPR/Cas9 system.

For the *in situ* knock-in *degron::ego-1*(*ust614*) transgene, the injection mixture contained PDD162 (50 ng μL^{-1}), the *degron::ego-1* repair plasmid (50 ng μL^{-1}), pCFJ90 (5 ng μL^{-1}), and three sgRNAs (30 ng μL^{-1}). The mixture was injected into young adult CA1199 (*sun-1p*::TIR1::mRuby::sun-1 3′UTR) animals. The transgenes were integrated via the CRISPR/Cas9 method.

For ectopic transgenes, the injection mixture contained pDD162 (50 ng μL^{-1}), an ectopic transgene homology-directed repair plasmid (50 ng μL^{-1}), pCFJ90 (5 ng μL^{-1}), and three or four sgRNAs (30 ng μL^{-1}). The mixture was injected into young adult N2 animals. The transgenes were integrated by the modified counterselection (cs)-CRISPR method (Chen et al., 2018; Frøkjær-Jensen et al., 2008).

The sgRNAs used in this study for transgene construction are listed in Supplementary Table S3.

Imaging and quantification

Images were collected using a Leica DM4B microscope with a Leica Thunder image processing system.

To quantify embryos exhibiting perinuclear GFP::NRDE-3 foci, an embryo was defined as positive if one or more NRDE-3 foci were observed. The number of embryos analyzed is indicated at

the corresponding positions in the figures. The bar graph displays the percentage of NRDE-3 foci-positive embryos.

RNAi

RNAi experiments were performed at 20°C as described previously (Timmons et al., 2001). HT115 bacteria expressing the empty vector L4440 (a gift from A. Fire) were used as controls. Bacterial clones expressing dsRNAs were obtained from the Ahringer RNAi library and sequenced to verify their identity. Images were collected using a Leica DM4 B microscope.

For *lir-1* RNAi, *lir-1* and *lin-26* are cotranscribed in an operon, and *lir-1* mutant is viable, whereas loss of *lin-26* results in larval lethality. RNAi targeting *lir-1* is lethal, indicating that RNAi silences *lir-1*/*lin-26* polycistronic RNA in nucleus by nuclear RNAi pathway. Synchronized embryos were placed on feeding plates.

For RNAi targeting centriole and PCM genes, synchronized embryos were hatched and cultured on NGM plates for 41 h. L4 animals were transferred to RNAi plates and F_1 embryos were imaged.

Quantitative real-time PCR

Worm samples from the indicated animals were collected and digested at 65°C with proteinase K to extract genomic DNA. qRT–PCR was performed using a MyIQ2 real-time PCR machine (Bio-Rad) with AceQ SYBR Green Master mix (Vazyme). The primers used for qRT–PCR are listed in Supplementary Table S4.

Auxin treatment

Unless otherwise indicated, auxin treatment was performed by transferring worms to bacteria-seeded plates containing auxin. The natural auxin indole-3-acetic acid (IAA) was purchased from Sigma–Aldrich (#12886). A 400 mmol L^{-1} stock solution in ethanol was prepared and stored at 4°C for up to one month. IAA was diluted into NGM agar and cooled to approximately 50°C before being added to the plates. Fresh OP50 spreading plates. The plates were left at room temperature for 1–2 days to allow bacterial lawn growth. For all IAA treatments, 0.25% ethanol was used as a control.

For all strains containing *degron::ego-1*(*ust614*);*sun-1p::*TIR1::mRuby::sun-1 3′UTR, animals exposed to IAA treatment exhibited degradation of degron-tagged EGO-1 in the germline, leading to embryonic arrest in F_1 embryos. For *degron::ego-1*(*ust614*);*sun-1p::*TIR1::mRuby::sun-1 3′UTR; 3xFLAG::GFP::NRDE-3(ust574, KI), *eri-1*(*mg366*);*rrf-1*(*pk1417*);*rrf-2*(*ok210*); 3xFLAG::GFP::NRDE-3(ust574, KI) and *drh-3*(*ne4253*);*degron::tbb-2*(*ust672*);*sun-1p::*TIR1::mRuby::sun-1 3′UTR;3xFLAG::GFP::NRDE-3(*ust574*, KI), synchronized embryos were exposed onto NGM plates seeded with OP50 and containing 1 mmol L^{-1} IAA. For *rrf-1*(*pk1417*);*rrf-2*(*ok210*);*degron::ego-1*(*ust614*);*sun-1p::*TIR1::mRuby::sun-1 3′UTR; 3xFLAG::GFP::NRDE-3(ust574, KI) and *eri-1*(*mg366*);*rrf-1*(*pk1417*);*rrf-2*(*ok210*);*degron::ego-1*(*ust614*);*sun-1p::*TIR1::mRuby::sun-1 3′UTR;3xFLAG::GFP::NRDE-3(ust574, KI), synchronized animals were grown on OP50 on NGM plates and at the L4 stage, they were transferred to NGM plates containing 1 mmol L^{-1} IAA. Pictures were taken 48 h after IAA treatment.

Actinomycin D treatment

Actinomycin D (MedChemExpress, catalog No. HY-17559, CAS: 50-76-0) was prepared as a stock solution in DMSO at a concentration of 50 mg mL^{-1}. The stock solution was diluted to final concentrations ranging from 5 to 30 μg mL^{-1} with concentrated OP50. NGM plates were prepared and incubated at room temperature overnight prior to use. Synchronized L4-stage worms were transferred to the seeded plates and grown for 24 h before imaging.

Cold-shock assay

Synchronized hermaphrodites on day 1 of adulthood were transferred to new NGM plates and incubated at 4°C or 15°C for 12 h. Subsequently, the worms were allowed to recover for 1 h at 20°C before imaging.

Heat-shock assay

Synchronized hermaphrodites on day 1 of adulthood were transferred to new NGM plates and incubated at 25°C or 37°C for 12 h. After that, the worms were allowed to recover for 1 h at 20°C before imaging.

Starvation assay

Synchronized hermaphrodites on day 1 of adulthood were transferred to empty NGM plates without any bacterial lawn for 12 h and then imaged. Alternatively, starved worms were transferred to NGM plates with bacteria for 1 h before imaging.

Brood size

Synchronized L4 hermaphrodites were singled onto NGM plates and transferred daily as adults until embryo production ceased. The total number of progenies produced was then counted.

Hatch ratio

Synchronized adult hermaphrodites were transferred to NGM plates to lay eggs, which were subsequently removed. The numbers of embryos and hatched larvae were scored, and the hatch ratio was calculated as the number of hatched larvae divided by the total number of embryos.

Development rate

Synchronized adult hermaphrodites were transferred to NGM plates to lay eggs, which were subsequently removed. The growth of the progeny was monitored every 24 h at 20°C.

RNA immunoprecipitation (RIP) assay

3xFLAG::GFP::NRDE-3(ust574, KI), 3xFLAG::GFP::NRDE-3 (ggIS1, bombardment) and NRDE-3(*NLS)-associated siRNAs were isolated from embryo lysates. The embryos were cryo-grolded in lysis buffer (20 mmol L^{-1} Tris-HCl, pH 7.5, 200 mmol L^{-1} NaCl, 2.5 mmol L^{-1} $MgCl_2$, 0.5% NP-40, and 10% glycerol) supplemented with proteinase inhibitor tablets (Roche). The lysate was precleared with protein G-agarose beads (Roche) and

https://doi.org/10.1007/s11427-024-2818-7

then incubated with anti-FLAG M2 magnetic beads (Sigma #M8823). The beads were washed extensively and eluted with 3xFLAG peptide (Sigma #F4799). The eluates were incubated with DNase I followed by TRIzol purification and isopropanol precipitation. The precipitated RNA was treated with RNA 5′ polyphosphatase (Biosearch) and re-extracted with TRIzol reagent.

TBB-2-associated siRNAs were isolated from *mex5p*::3xHA::tagRFP::TBB-2; GFP::NRDE-3(*NLS) embryo lysates and incubated with anti-HA magnetic beads (Thermo Scientific #88836). The beads were washed extensively and eluted with HA peptide (Thermo Scientific #26184).

siRNA deep sequencing

NRDE-3- and TBB-2-bound siRNAs were subjected to deep sequencing using an Illumina platform by Novogene Bioinformatics Technology Co., Ltd., for library preparation and sequencing. Briefly, 3′ and 5′ adaptors were ligated to the 3′ and 5′ ends of small RNAs, respectively. After purification and size selection, libraries with insertions between 18–30 bp were subjected to deep sequencing.

The Illumina-generated raw reads were first filtered to remove adaptors, low-quality tags, and contaminants to obtain clean reads at BGI Shenzhen. Clean reads ranging from 18 to 30 nt were mapped to the unmasked *C. elegans* genome and the transcriptome assembly WS243, respectively, using Bowtie2 with default parameters. The number of reads targeting each transcript was counted using custom Perl scripts and displayed by IGV.

Metagene analysis

The metagene profiles were generated according to a method described previously (Singh et al., 2021). The BigWig files were generated using the Snakemake workflow (https://gitlab.Pasteur.fr/bli/bioinfo_utils). Briefly, the 3′ adapters and 5′ adapters were trimmed from the raw reads using Cutadapt v.1.18 with the following parameters: -a AGATCGGAAGAGCACACGTCT-g GTTCAGAGTTCTACAGTCCGACGATC–discard-untrimmed. After adapter trimming, the reads containing 18 to 26 nt were selected using Bioawk. The selected 18–26 nucleotide reads were aligned to the *C. elegans* genome (ce11, *C. elegans* Sequencing Consortium WBcel235) using Bowtie2 v.2.3.4.3 with the following parameters: -L 6 -i S,1,0.8 -N 0. The resulting alignments were used to generate bigwig files with a custom bash script using BEDtools version v2.27.1, BEDOPS version 2.4.35, and bedGraphToBigWig version 4. Read counts in the bigwig file were normalized to million "nonstructural" mappers —that is, reads containing 18 to 26 nt and mapped to annotations not belonging to "structural" (tRNA, snRNA, snoRNA, rRNA, ncRNA) categories—and counted using featureCounts77 v.1.6.3. These bigwig files were used to generate "metaprofiles" files with a shell script.

Statistics

The means and standard deviations of the results are presented in bar graphs with error bars. All experiments were conducted with independent *C. elegans* animals at the indicated number (N) of times. Statistical analysis was performed with two-tailed Student's *t*-tests.

Data availability

The data that support this study are available from the corresponding author upon request. All the high-throughput data generated by this work have been deposited in the Genome Sequence Archive (Genomics, Proteomics & Bioinformatics 2021) (Chen et al., 2021) in National Genomics Data Center (Nucleic Acids Res 2022) (Xue et al., 2022), China National Center for Bioinformation/Beijing Institute of Genomics, Chinese Academy of Sciences (GSA: CRA017153) that are publicly accessible at https://ngdc.cncb.ac.cn/gsa/ CRA017153.

Compliance and ethics

The authors declare that they have no conflict of interest.

Acknowledgement

We are grateful to members of the Guang laboratory and Dr. Carolyn Phillips' laboratory for their comments. We are grateful to the International *C. elegans* Gene Knockout Consortium and the National Bioresource Project for providing the strains. Some strains were provided by the CGC, which is funded by the National Institutes of Health (NIH) Office of Research Infrastructure Programs (P40 OD010440). This work was supported by grants from the National Natural Science Foundation of China (32230016 awarded to S.G., 32270583 awarded to C. Z., 32070619 awarded to X.F., 2023M733425 awarded to X.H., and 32300438 awarded to X.H.), the National Key R&D Program of China (2022YFA1302700 to S.G.), the Research Funds of Center for Advanced Interdisciplinary Science and Biomedicine of IHM (QYPY20230021 awarded to S.G.) and the Fundamental Research Funds for the Central Universities.

Supporting information

The supporting information is available online at https://doi.org/10.1007/s11427-024-2818-7. The supporting materials are published as submitted, without typesetting or editing. The responsibility for scientific accuracy and content remains entirely with the authors.

References

Alliegro, M.C., and Alliegro, M.A. (2008). Centrosomal RNA correlates with intron-poor nuclear genes in *Spisula* oocytes. Proc Natl Acad Sci USA 105, 6993–6997.

Alliegro, M.C., Alliegro, M.A., and Palazzo, R.E. (2006). Centrosome-associated RNA in surf clam oocytes. Proc Natl Acad Sci USA 103, 9034–9038.

Barrière, A., and Bertrand, V. (2022). Labelling of active transcription sites with argonaute NRDE-3—image active transcription sites *in vivo* in *Caenorhabditis elegans*. BIO-PROTOCOL 12, e4427.

Bergalet, J., Patel, D., Legendre, F., Lapointe, C., Benoit Bouvrette, L.P., Chin, A., Blanchette, M., Kwon, E., and Lécuyer, E. (2020). Inter-dependent centrosomal co-localization of the cen and ik2 cis-natural antisense mRNAs in *Drosophila*. Cell Rep 30, 3339–3352.e6.

Bernstein, E., Caudy, A.A., Hammond, S.M., and Hannon, G.J. (2001). Role for a bidentate ribonuclease in the initiation step of RNA interference. Nature 409, 363–366.

Billi, A.C., Fischer, S.E., and Kim, J.K. (2014). Endogenous RNAi pathways in *C. elegans*. WormBook 7, 1–49.

Blower, M.D., Feric, E., Weis, K., and Heald, R. (2007). Genome-wide analysis demonstrates conserved localization of messenger RNAs to mitotic microtubules. J Cell Biol 179, 1365–1373.

Bobinnec, Y., Fukuda, M., and Nishida, E. (2000). Identification and characterization of *Caenorhabditis elegans* γ-tubulin in dividing cells and differentiated tissues. J Cell Sci 113, 3747–3759.

Bosher, J.M., Dufourcq, P., Sookhareea, S., and Labouesse, M. (1999). RNA interference can target pre-mRNA: consequences for gene expression in a *Caenorhabditis elegans* operon. Genetics 153, 1245–1256.

Burton, N.O., Burkhart, K.B., and Kennedy, S. (2011). Nuclear RNAi maintains heritable gene silencing in *Caenorhabditis elegans*. Proc Natl Acad Sci USA 108, 19683–19688.

Castel, S.E., and Martienssen, R.A. (2013). RNA interference in the nucleus: roles for small RNAs in transcription, epigenetics and beyond. Nat Rev Genet 14, 100–112.

Chen, T., Chen, X., Zhang, S., Zhu, J., Tang, B., Wang, A., Dong, L., Zhang, Z., Yu, C., Sun, Y., et al. (2021). The genome sequence archive family: toward explosive data growth and diverse data types. Genomics Proteomics BioInf 19, 578–583.

Chen, X., Liao, S., Huang, X., Xu, T., Feng, X., and Guang, S. (2018). Targeted chromosomal rearrangements via combinatorial use of CRISPR/Cas9 and Cre/*LoxP* technologies in *Caenorhabditis elegans*. G3 Genes|Genomes|Genet 8, 2697–

2707.
Chen, X., Zhang, D., Su, N., Bao, B., Xie, X., Zuo, F., Yang, L., Wang, H., Jiang, L., Lin, Q., et al. (2019). Visualizing RNA dynamics in live cells with bright and stable fluorescent RNAs. Nat Biotechnol 37, 1287–1293.
Chen, X., Wang, K., Mufti, F.U.D., Xu, D., Zhu, C., Huang, X., Zeng, C., Jin, Q., Huang, X., Yan, Y., et al. (2024). Germ granule compartments coordinate specialized small RNA production. Nat Commun 15, 5799.
Chouaib, R., Safieddine, A., Pichon, X., Imbert, A., Kwon, O.S., Samacoits, A., Traboulsi, A.M., Robert, M.C., Tsanov, N., Coleno, E., et al. (2020). A dual protein-mRNA localization screen reveals compartmentalized translation and widespread co-translational RNA targeting. Dev Cell 54, 773–791.e5.
Cogoni, C., and Macino, G. (1999). Gene silencing in *Neurospora crassa* requires a protein homologous to RNA-dependent RNA polymerase. Nature 399, 166–169.
Fang, J., and Lerit, D.A. (2022). Orb-dependent polyadenylation contributes to PLP expression and centrosome scaffold assembly. Development 149, dev200426.
Fire, A., Xu, S.Q., Montgomery, M.K., Kostas, S.A., Driver, S.E., and Mello, C.C. (1998). Potent and specific genetic interference by double-stranded RNA in *Caenorhabditis elegans*. Nature 391, 806–811.
Fischer, S.E.J., and Ruvkun, G. (2020). *Caenorhabditis elegans* ADAR editing and the ERI-6/7/MOV10 RNAi pathway silence endogenous viral elements and LTR retrotransposons. Proc Natl Acad Sci USA 117, 5987–5996.
Frøkjær-Jensen, C., Wayne Davis, M., Hopkins, C.E., Newman, B.J., Thummel, J.M., Olesen, S.P., Grunnet, M., and Jorgensen, E.M. (2008). Single-copy insertion of transgenes in *Caenorhabditis elegans*. Nat Genet 40, 1375–1383.
Guang, S., Bochner, A.F., Burkhart, K.B., Burton, N., Pavelec, D.M., and Kennedy, S. (2010). Small regulatory RNAs inhibit RNA polymerase II during the elongation phase of transcription. Nature 465, 1097–1101.
Guang, S., Bochner, A.F., Pavelec, D.M., Burkhart, K.B., Harding, S., Lachowiec, J., and Kennedy, S. (2008). An argonaute transports siRNAs from the cytoplasm to the nucleus. Science 321, 537–541.
Hombach, S., and Kretz, M. (2016). Non-coding RNAs: classification, biology and functioning. Adv Exp Med Biol. 937, 3–17.
Honda, Y., Tsuchiya, K., Sumiyoshi, E., Haruta, N., and Sugimoto, A. (2017). Tubulin isotype substitution revealed that isotype combination modulates microtubule dynamics in *C. elegans* embryos. J Cell Sci 130, 1652–1661.
Huang, K., Chen, X., Li, C., Song, Q., Li, H., Zhu, L., Yang, Y., and Ren, A. (2021). Structure-based investigation of fluorogenic *Pepper aptamer*. Nat Chem Biol 17, 1289–1295.
Hurd, D.D. (2018). Tubulins in *C. elegans*. WormBook 1–32.
Jiang, L., Xie, X., Su, N., Zhang, D., Chen, X., Xu, X., Zhang, B., Huang, K., Yu, J., Fang, M., et al. (2023). Large stokes shift fluorescent RNAs for dual-emission fluorescence and bioluminescence imaging in live cells. Nat Methods 20, 1563–1572.
Jie, M., Feng, T., Huang, W., Zhang, M., Feng, Y., Jiang, H., and Wen, Z. (2021). Subcellular localization of miRNAs and implications in cellular homeostasis. Genes 12, 856.
Lambert, J.D., and Nagy, L.M. (2002). Asymmetric inheritance of centrosomally localized mRNAs during embryonic cleavages. Nature 420, 682–686.
Lécuyer, E., Yoshida, H., Parthasarathy, N., Alm, C., Babak, T., Cerovina, T., Hughes, T.R., Tomancak, P., and Krause, H.M. (2007). Global analysis of mRNA localization reveals a prominent role in organizing cellular architecture and function. Cell 131, 174–187.
Lee, R.C., Hammell, C.M., and Ambros, V. (2006). Interacting endogenous and exogenous RNAi pathways in *Caenorhabditis elegans*. RNA 12, 589–597.
Lerit, D.A. (2022). Signed, sealed, and delivered: RNA localization and translation at centrosomes. Mol Biol Cell 33, pe3.
Lewis, A., Berkyurek, A.C., Greiner, A., Sawh, A.N., Vashisht, A., Merrett, S., Flamand, M.N., Wohlschlegel, J., Sarov, M., Miska, E.A., et al. (2020). A family of argonaut-interacting proteins gates nuclear RNAi. Mol Cell 78, 862–875.e8.
Liao, S., Chen, X., Xu, T., Jin, Q., Xu, Z., Xu, D., Zhou, X., Zhu, C., Guang, S., and Feng, X. (2021). Antisense ribosomal siRNAs inhibit RNA polymerase I-directed transcription in *C. elegans*. Nucleic Acids Res 49, 9194–9210.
Liu, L., Wang, X., Zhao, W., Li, Q., Li, J., Chen, H., and Shan, G. (2023). Systematic characterization of small RNAs associated with *C. elegans* Argonautes. Sci China Life Sci 66, 1303–1322.
Lorson, M.A., Horvitz, H.R., and van den Heuvel, S. (2000). LIN-5 is a novel component of the spindle apparatus required for chromosome segregation and cleavage plane specification in *Caenorhabditis elegans*. J Cell Biol 148, 73–86.
Mao, H., Zhu, C., Zong, D., Weng, C., Yang, X., Huang, H., Liu, D., Feng, X., and Guang, S. (2015). The Nrde pathway mediates small-RNA-directed histone H3 lysine 27 trimethylation in *Caenorhabditis elegans*. Curr Biol 25, 2398–2403.
Nishida, K., Tsuchiya, K., Obinata, H., Onodera, S., Honda, Y., Lai, Y.C., Haruta, N., and Sugimoto, A. (2021). Expression patterns and levels of all tubulin isotypes analyzed in GFP knock-in *C. elegans* strains. Cell Struct Funct 46, 51–64.
Padeken, J., Methot, S., Zeller, P., Delaney, C.E., Kalck, V., and Gasser, S.M. (2021). Argonaute NRDE-3 and MBT domain protein LIN-61 redundantly recruit an H3K9me3 HMT to prevent embryonic lethality and transposon expression. Genes Dev 35, 82–101.
Pak, J., and Fire, A. (2007). Distinct populations of primary and secondary effectors during RNAi in *C. elegans*. Science 315, 241–244.
Phillips, C.M., Montgomery, T.A., Breen, P.C., and Ruvkun, G. (2012). MUT-16 promotes formation of perinuclear *Mutator* foci required for RNA silencing in the *C. elegans* germline. Genes Dev 26, 1433–1444.
Phillips, C.M., and Updike, D.L. (2022). Germ granules and gene regulation in the *Caenorhabditis elegans* germline. Genetics 220, iyab195.
Pintard, L., and Bowerman, B. (2019). Mitotic cell division in *Caenorhabditis elegans*. Genetics 211, 35–73.
Raff, J.W., Whitfield, W.G.F., and Glover, D.M. (1990). Two distinct mechanisms localise cyclin B transcripts in syncytial *Drosophila* embryos. Development 110, 1249–1261.
Ryder, P.V., Fang, J., and Lerit, D.A. (2020). centrocortin RNA localization to centrosomes is regulated by FMRP and facilitates error-free mitosis. J Cell Biol 219, e202004101.
Ryder, P.V., and Lerit, D.A. (2018). RNA localization regulates diverse and dynamic cellular processes. Traffic 19, 496–502.
Safieddine, A., Coleno, E., Salloum, S., Imbert, A., Traboulsi, A.M., Kwon, O.S., Lionneton, F., Georget, V., Robert, M.C., Gostan, T., et al. (2021). A choreography of centrosomal mRNAs reveals a conserved localization mechanism involving active polysome transport. Nat Commun 12, 1352.
Saikia, B.J., Bhardwaj, J., Paul, S., Sharma, S., Neog, A., Paul, S.R., and Bk, B. (2023). Understanding the roles and regulation of mitochondrial microRNAs (MitomiRs) in neurodegenerative diseases: current status and advances. Mech Ageing Dev 213, 111838.
Sepulveda, G., Antkowiak, M., Brust-Mascher, I., Mahe, K., Ou, T., Castro, N.M., Christensen, L.N., Cheung, L., Jiang, X., Yoon, D., et al. (2018). Co-translational protein targeting facilitates centrosomal recruitment of PCNT during centrosome maturation in vertebrates. eLife 7, e34959.
Seroussi, U., Lugowski, A., Wadi, L., Lao, R.X., Willis, A.R., Zhao, W., Sundby, A.E., Charlesworth, A.G., Reinke, A.W., and Claycomb, J.M. (2023). A comprehensive survey of *C. elegans* argonaute proteins reveals organism-wide gene regulatory networks and functions. eLife 12, e83853.
Shimomura, O. (2005). The discovery of aequorin and green fluorescent protein. J Microsc 217, 3–15.
Shukla, A., Yan, J., Pagano, D.J., Dodson, A.E., Fei, Y., Gorham, J., Seidman, J.G., Wickens, M., and Kennedy, S. (2020). poly(UG)-tailed RNAs in genome protection and epigenetic inheritance. Nature 582, 283–288.
Sijen, T., Fleenor, J., Simmer, F., Thijssen, K.L., Parrish, S., Timmons, L., Plasterk, R.H. A., and Fire, A. (2001). On the role of RNA amplification in dsRNA-triggered gene silencing. Cell 107, 465–476.
Singh, M., Cornes, E., Li, B., Quarato, P., Bourdon, L., Dingli, F., Loew, D., Proccacia, S., and Cecere, G. (2021). Translation and codon usage regulate Argonaute slicer activity to trigger small RNA biogenesis. Nat Commun 12, 3492.
Smardon, A., Spoerke, J.M., Stacey, S.C., Klein, M.E., Mackin, N., and Maine, E.M. (2000). EGO-1 is related to RNA-directed RNA polymerase and functions in germline development and RNA interference in *C.elegans*. Curr Biol 10, 169–178.
Strome, S., Powers, J., Dunn, M., Reese, K., Malone, C.J., White, J., Seydoux, G., Saxton, W., and Salmon, T. (2001). Spindle dynamics and the role of γ-tubulin in early *Caenorhabditis elegans* embryos. Mol Biol Cell 12, 1751–1764.
Timmons, L., Court, D.L., and Fire, A. (2001). Ingestion of bacterially expressed dsRNAs can produce specific and potent genetic interference in *Caenorhabditis elegans*. Gene 263, 103–112.
Toudji-Zouaz, A., Bertrand, V., and Barrière, A. (2021). Imaging of native transcription and transcriptional dynamics *in vivo* using a tagged Argonaute protein. Nucleic Acids Res 49, e86.
Tsien, R.Y. (1998). The green fluorescent protein. Annu Rev Biochem 67, 509–544.
Wolff, I.D., Tran, M.V., Mullen, T.J., Villeneuve, A.M., Wignall, S.M., and Strome, S. (2016). Assembly of *Caenorhabditis elegans* acentrosomal spindles occurs without evident microtubule-organizing centers and requires microtubule sorting by KLP-18/kinesin-12 and MESP-1. Mol Biol Cell 27, 3122–3131.
Xu, F., Feng, X., Chen, X., Weng, C., Yan, Q., Xu, T., Hong, M., and Guang, S. (2018). A cytoplasmic Argonaute protein promotes the inheritance of RNAi. Cell Rep 23, 2482–2494.
Xu, K., Li, Z., Mao, L., Guo, Z., Chen, Z., Chai, Y., Xie, C., Yang, X., Na, J., Li, W., et al. (2024). AlphaFold2-guided engineering of split-GFP technology enables labeling of endogenous tubulins across species while preserving function. PLoS Biol 22, e3002615.
Xue, Y., Bao, Y., Zhang, Z., Zhao, W., Xiao, J., He, S., Zhang, G., Li, Y., Zhao, G., Chen, R., et al. (2022). Database resources of the National Genomics Data Center, China

National Center for bioinformation in 2022. Nucleic Acids Res 50, D27–D38.
Zein-Sabatto, H., and Lerit, D.A. (2021). The identification and functional analysis of mRNA localizing to centrosomes. Front Cell Dev Biol 9, 782802.
Zhang, L., Ward, J.D., Cheng, Z., and Dernburg, A.F. (2015). The auxin-inducible degradation (AID) system enables versatile conditional protein depletion in *C. elegans*. Development dev.129635.
Zhou, X., Feng, X., Mao, H., Li, M., Xu, F., Hu, K., and Guang, S. (2017). RdRP-synthesized antisense ribosomal siRNAs silence pre-rRNA via the nuclear RNAi pathway. Nat Struct Mol Biol 24, 258–269.
Zhou, X., Xu, F., Mao, H., Ji, J., Yin, M., Feng, X., and Guang, S. (2014). Nuclear RNAi contributes to the silencing of off-target genes and repetitive sequences in *Caenorhabditis elegans*. Genetics 197, 121–132.
Zhu, C., Yan, Q., Weng, C., Hou, X., Mao, H., Liu, D., Feng, X., and Guang, S. (2018). Erroneous ribosomal RNAs promote the generation of antisense ribosomal siRNA. Proc Natl Acad Sci USA 115, 10082–10087.
Zhuang, J.J., Banse, S.A., and Hunter, C.P. (2013). The nuclear Argonaute NRDE-3 contributes to transitive RNAi in *Caenorhabditis elegans*. Genetics 194, 117–131.
Zuo, F., Jiang, L., Su, N., Zhang, Y., Bao, B., Wang, L., Shi, Y., Yang, H., Huang, X., Li, R., et al. (2024). Imaging the dynamics of messenger RNA with a bright and stable green fluorescent RNA. Nat Chem Biol 20, 1272–1281.